Ion collection by a sphere in a flowing plasma: 2. non-zero Debye length

2003 Plasma Phys. Control. Fusion 45 1477

(http://iopscience.iop.org/0741-3335/45/8/307)

INSTITUTE OF PHYSICS PUBLISHING PLASMA PHYSICS AND CONTROLLED FUSION

Plasma Phys. Control. Fusion **45** (2003) 1477–1500 PII: S0741-3335(03)63101-5

Ion collection by a sphere in a flowing plasma: 2. non-zero Debye length

I H Hutchinson

Plasma Science and Fusion Center, Massachusetts Institute of Technology, Cambridge, MA, USA

Received 7 May 2003
Published 17 July 2003
Online at stacks.iop.org/PPCF/45/1477

Abstract

The spatial distribution of ion flux to a sphere in a flowing collisionless plasma is calculated using a particle-in-cell code SCEPTIC. The code is validated by comparing with prior stationary-plasma and approximate calculations. Comprehensive results are provided for ion temperatures 1 and 0.1 times the electron temperature, and for Debye length from 0.01 to 100 times the probe size. A remarkable qualitatively new result is obtained: over a range of Debye lengths from roughly 0.1 to 10 times the probe radius at $T_i = 0.1T_e$, the downstream side of the probe receives substantially higher flux density than the upstream side when the flow is subsonic. This unexpected reversal of the asymmetry reinforces the need for these fully self-consistent calculations, but renders the use of the flux ratio for Mach-probe purposes problematic, even for deriving the direction of the flow.

1. Introduction

In an earlier paper, which is referred to hereafter as paper 1 [1], the specialized coordinate electrostatic particle and thermals in cell (SCEPTIC) code was described and used to solve the long-unsolved problem of the interaction of an ion-collecting sphere with a flowing collisionless quasineutral plasma. Quasineutrality holds when the Debye length is zero—negligible compared with the probe radius. Here, the results of using the SCEPTIC code to solve the more realistic problem of non-zero Debye length are reported.

The calculation is important for a number of plasma applications. The author's main motivation was to understand Mach probes—Langmuir probes configured to measure the flow speed by using separate ion collectors facing upstream and downstream. Although the dependence of the upstream/downstream flux ratio on velocity has been solved for magnetized probes (whose dimensions are larger than the ion Larmor radius) [2–4] it has not previously been solved for unmagnetized probes, even though a number of experiments have begun to use them [5–8]. Some experimental interpretation has relied on a heuristic formula of Hudis and Lidsky [9], but the formula is based on a one-dimensional approach which is unphysical [10]. It is also quantitatively incorrect, as was shown in paper 1, which gave a calibration factor that

is correct for zero Debye length. While paper 1 is rigorously correct in its assumptions, the present results show that non-zero Debye lengths give rise to numerically important differences even when λ_{De} is as small as a few per cent of the probe radius, and it gives rise to dramatic qualitative differences at higher values.

The problem of charging of spherical dust grains in a plasma is of great current interest and is governed by the ion collection flux (see, e.g. [11, 12]). Moreover, in experiments grains usually reside in regions where the plasma is flowing at a substantial fraction of the speed of sound. The present calculations idealize such situations, because here the distant plasma is taken as uniform, whereas experimental grains are usually in strong gradient regions. Nevertheless, the calculations represent a substantial step forward in investigating this problem, relative to the usual assumption based on orbit motion limited (OML) collection, neglecting flow. The angular dependence of the flux is most important for electrically insulating grains but the present calculations take the sphere to be an equipotential, which is assured only for conducting grains. The problem of self-consistent surface potential variation for a nonconducting grain is left for future work.

Satellite interactions with space plasmas are often at quite high Mach numbers (typically 8 in low earth orbit). Such speeds result in very low plasma collection on the downstream side. Perhaps because of that, prior calculations of ion collection have generally neglected the angular dependence of ion collection. The present results remedy that situation and provide information that may be useful for tethers [13] as well as satellites themselves.

Of course, this study has limitations for practical applications. The complete neglect of magnetic field is an idealization that might change the result; so it would be helpful in future to explore the effects of large but finite ion Larmor radius. Collisions, neglected here, are also known to have a significant effect in some symmetric cases. It seems likely that in a flowing plasma, where particle angular momentum is not conserved, the effects of collisions may not be so important, but that remains to be demonstrated.

The operational principles of SCEPTIC are summarized in section 2, the reader being referred to paper 1 for a fuller explanation. Only those aspects that are specific to the non-zero Debye length case are described in detail. The most challenging problems relate to the outer mesh boundary conditions which are described in section 3, and validated by comparison with orbital integration. In section 4 the code is further validated by benchmarking against the stationary plasma calculations of Laframboise [14, 15] for a large range of λ_{De}. Comparison with prior approximate calculations and with experiments illustrates the magnitude of their discrepancies from the ideal case. New results are described in section 5. The plasma behaviour is surveyed for the range of parameters and systematic numerical results are presented for the collected flux and its upstream/downstream ratio.

2. Equations and solution method

Each ion, of charge Ze and mass m, at position $\boldsymbol{x}$ is governed by the equation of motion in the electrostatic potential:

$$m\frac{\mathrm{d}^2\boldsymbol{x}}{\mathrm{d}t^2} = -Ze\nabla\phi. \tag{1}$$

The electrons are taken to have density

$$n_e = Zn_{i\infty}\exp\left(\frac{e\phi}{T_e}\right), \tag{2}$$

where $n_{i\infty}$ is the ion density where $\phi = 0$, far from the probe.

The self-consistent potential satisfies Poisson's equation:

$$\nabla^2\phi = \frac{e}{\epsilon_0}(n_e - Zn_i), \tag{3}$$

where the ion density n_i is obtained by integration over all velocities of the ion distribution function, $f(\boldsymbol{x}, \boldsymbol{v})$ which is represented by the large number of individual ions in the calculation.

It is convenient to measure potential in units of T_e/e, velocity in units of $(ZT_e/m)^{1/2}$, density in units of $n_{i\infty}$ and to take the probe radius as $r = 1$, effectively making the units of time equal to the probe radius divided by $(ZT_e/m)^{1/2}$. These choices undimensionalize the problem, but for simplicity, we shall continue to use the same symbols for the dimensionless quantities. The dimensionless Poisson equation, for example, is

$$\nabla^2\phi = \frac{1}{\lambda_{\mathrm{De}}^2}(\mathrm{e}^{\phi} - n_i), \tag{4}$$

where λ_{De} is the electron Debye length at infinity, $(\epsilon_0 T_e/e^2 n_e)^{1/2}$. Notice that the velocity is normalized to a value that is somewhat less than the ion sound speed ($c_s = [(ZT_e+3T_i)/m]^{1/2}$) when the ion temperature is non-zero. But the normalization factor $(ZT_e/m)^{1/2}$ is well defined and independent of position, unlike c_s.

The code uses a standard particle-in-cell (PIC) approach except that the cell mesh for potential is spherical, even though particles are advanced in Cartesian coordinates, as described in paper 1. The differences for non-zero Debye length are that simple uniformly spaced finite differences in the radial direction are used for Debye length greater than 10^{-2}, and that the full Poisson differential equation must be solved. That solution is obtained with a successive overrelaxation scheme using Chebychev acceleration [16]. The degree of overrelaxation is adjusted in a semi-implicit scheme accounting for the exponential electron density variation. As a result, at small Debye length, where the scheme approximates a direct Newton-method solver, the convergence is extremely rapid, while at large Debye length the convergence rate is much slower, equivalent to the optimized SOR rate. However, in the latter case, the potential hardly changes from step to step, so the initial potential guess from the previous step is so good that satisfactory convergence is still rapidly achieved.

The total number of particles in the simulation region is kept constant and particles that leave the region by crossing a boundary are immediately reinjected in a manner discussed in section 3. The number of particles advanced per processor can be chosen to be large enough so that the potential solving step, which is done on only the master node of the multiprocessor (MPI) version, is a small fraction of the total computing cost. With a master node somewhat faster than the slaves, the result is that the computation uses the full cpu capacity of the slaves. At 200 k particles per processor, several steps per second of elapsed time are achieved on 1200 MHz Athlon processors. Typically 500–1000 steps are sufficient to reach equilibrium. Both nearest-grid-point (NGP) and cloud-in-cell (CIC) [17,18] versions are available, which are useful for numerical validation, but all results shown here use a CIC version. Approximately, 7 million particles (200 k on each of 35 processors) are used, which gives excellent statistical accuracy on a 100 (radial) by 30 (angular) mesh covering typically $1 \leqslant r \leqslant 5$. At small Debye length, the radial mesh number must be increased—up to 500 is still quite satisfactory—and for greater angular resolution 100 angular cells have been used.

3. Boundary conditions

In the quasineutral case of paper 1, the major boundary condition difficulty arose from the singularity at the probe. In the present case, provided the radial mesh spacing exceeds the Debye length, no difficulty occurs at the probe boundary, since the sheath itself is now resolved.

Instead major difficulties arise with the handling of the outer boundary of the computational region.

In the quasineutral case, the density perturbation at the outer boundary is rather small, and is well approximated by the asymptotic condition $\mathrm{d}\ln(n-n_\infty)/\mathrm{d}\ln r = -2$. Moreover, since the potential is given directly as a consequence of quasineutrality by the logarithm of the density, no boundary condition needs to be applied to the normalized potential ϕ. This latter fact also renders it unnecessary to relate the density in the modelled region to the actual value at infinity until the calculation is completed. The potential at the boundary is small, and it is a reasonable approximation to reinject particles with a distribution that reflects the flux in the distant unperturbed plasma.

In contrast, this full Poisson solution does not necessarily have small potential at the boundary. In the limit of large Debye length the potential is just $\phi(r) = \phi(1)/r$, which will be a significant fraction of the probe potential, since there are practical computational limits to the ratio of boundary to probe radius in the model. The potential is the solution of a second-order differential equation so it requires an outer boundary condition as well as an inner one. The density has to be calculated at each step, normalized to infinity, so that a means of calculating the effective n_∞ at each step is required. What is more, the asymptotic scaling of the density perturbation proportional to $1/r^2$ does not necessarily apply. And finally, because the potential is not small, it is not reasonable to reinject particles with distant distribution; instead, their acceleration up to the boundary edge must somehow be modelled. In general, such a model cannot be exact because it involves in principle knowledge of the potential profile in the outer region beyond the computational boundary, which has not been calculated.

Very *ad hoc* approaches to solving these problems have been adopted in previous studies. For example some simulations just increment the normal component of the velocity at the boundary to account for the energy increase in falling through the potential drop from infinity to the boundary. Such an expedient is physically equivalent to a step in potential at the boundary. This study has found such approaches to be inadequate.

In outline, the solution adopted for obtaining the boundary conditions in the SCEPTIC code consists of three parts, which will be explained in detail below. (1) The boundary condition on ϕ is obtained from an approximate analytic solution of the shielding equations for the outer region. (2) The distribution of reinjected particles is obtained from a solution of the orbit equations in the outer region, using the approximate analytic form for the potential profile, starting from a shifted Maxwellian distribution at 'infinity'. (3) The density at infinity is obtained from the measured boundary influx by an analytic relation.

3.1. Solution of shielding equations beyond the boundary

The asymptotic behaviour of the potential and density perturbation in the quasineutral regime proportional to r^{-2} can be traced to the effect of ion absorption by the probe. A point charge that absorbs no plasma particles gives rise (at small potentials) to the Debye–Hückel potential

$$\phi = \frac{\exp(-r/\lambda)}{r}, \tag{5}$$

where λ is the shielding length combining the electron and ion Debye lengths $\lambda^{-2} = \lambda_{\mathrm{De}}^{-2} + \lambda_{\mathrm{Di}}^{-2}$. The shielding can be considered to arise from a linearization of electron density governed by the Boltzmann factor $\exp(\phi)$ and the untrapped ion density $1 - \phi Z T_e/T_i$, both of which expressions can be derived from the Liouville theorem. (Inclusion of trapped ions gives the ions a Boltzmann factor like the electrons, but this differs from the OML value above only at higher order in ϕ than we consider.) The solution has exponential asymptotic decay, incorrect for a finite-sized probe.

When absorption of ions by the probe is accounted for, a modified form of Debye shielding applies as follows. The electrons have negligible depletion because they are assumed to be strongly repelled; their density remains Boltzmann as before. However, the ion phase space is unpopulated in regions whose orbits, when tracked backwards, intercept the probe. If we consider a place far from the probe, then minus the velocity of an unpopulated orbit must point within a small angle of the probe centre. The exact value of that limiting angle depends on the potential solution around the probe; for example, if there is an absorption radius (inside which all ions are collected) then the angle is given by the ratio of the absorption radius to the distance of the analysis point from the probe. It does not much matter what the exact limiting angle is, except that the solid angle that it subtends must be inversely proportional to the square of the probe distance, r^2. Consequently, the ion density perturbation caused by the unpopulated orbits is also inversely proportional to r^2 far from the probe.

Therefore, we can construct an appropriate generalization of the Debye shielding equation by expanding the Boltzmann exponentials for small ϕ in the usual way but including the ion depletion term proportional to r^{-2}, and retaining only terms that are first order in both ϕ and the fractional ion depletion:

$$\nabla^2\phi - \frac{\phi}{\lambda^2} = \frac{a}{r^2}, \tag{6}$$

where the constant a represents the density depletion due to collected orbits and can be written

$$a = \frac{r_b^2}{\lambda_{\mathrm{De}}^2}\,\frac{n_{i\infty}(1-\phi_b Z T_e/T_i) - n_{ib}}{n_{i\infty}} \tag{7}$$

with subscript b denoting values at the boundary. The linear inhomogeneous equation (6) for ϕ can be solved, assuming spherical symmetry, using a Green's function approach. For boundary conditions $\phi(r_b) = \phi_b$ and $\phi(\infty) = 0$, the solution is

$$\phi(r) = \phi_b \exp\left(\frac{r_b}{\lambda}\right) r_b\,\frac{\exp(-r/\lambda)}{r} + \frac{a\lambda}{2r}\left\{\mathrm{e}^{(2r_b-r)/\lambda}E_1(r_b/\lambda) - \mathrm{e}^{r/\lambda}E_1\left(\frac{r}{\lambda}\right) - \mathrm{e}^{-r/\lambda}\left[\mathrm{Ei}\left(\frac{r}{\lambda}\right) - \mathrm{Ei}\left(\frac{r_b}{\lambda}\right)\right]\right\}, \tag{8}$$

where $E_1(x) \equiv \int_x^\infty \exp(-s)/s\,\mathrm{d}s$ and $\mathrm{Ei}(x) = -E_1(-x)$ are exponential integral functions. Here, the first term is the standard Debye–Hückel expression, and the second term is the correction from the ion depletion: the contribution of the inhomogeneous term. (A form similar to equation (8) is derived in [19] p 211.)

The gradient of the potential at the boundary can therefore be written as:

$$\phi'(r_b) = -\left(\frac{1}{\lambda} + \frac{1}{r_b}\right)\phi(r_b) - \frac{a}{r_b}\exp\left(\frac{r_b}{\lambda}\right)E_1\left(\frac{r_b}{\lambda}\right), \tag{9}$$

which is the boundary condition on ϕ.

However, a numerical difficulty with this expression arises when r_b/λ is large, because the dominant terms then become the right-hand side, and amount to a specification on ϕ rather than ϕ'. Such a condition can become numerically inaccurate or even unstable when the ion temperature is low. Therefore, we note that in the limit $r_b/\lambda \gg 1$, the solution (8) becomes[1]

$$\phi \approx -\frac{a\lambda}{2r}\mathrm{e}^{r/\lambda}E_1\left(\frac{r}{\lambda}\right) \approx -\frac{a\lambda^2}{2r^2}, \tag{10}$$

which leads to $\phi' = -2\phi/r$. Therefore, the following somewhat *ad hoc* modification is used:

$$\phi'(r_b) = -\alpha\left[\left(\frac{1}{\lambda} + \frac{1}{r_b}\right)\phi(r_b) - \frac{a}{r_b}\exp\left(\frac{r_b}{\lambda}\right)E_1\left(\frac{r_b}{\lambda}\right)\right] - (1-\alpha)\frac{2\phi(r_b)}{r_b} \tag{11}$$

[1] By considering $r - r_b \gg \lambda$.

with

$$\alpha = \frac{1}{1 + (0.02 r_b/\lambda)^2}. \tag{12}$$

This expression yields the shielding form for all but very small values of λ.

3.2. Reinjection distribution orbit equations

To determine the distribution in position and velocity of the reinjected particles, accounting for non-zero potential at the boundary and drift velocity at infinity, requires an approximate solution of the orbit problem outside the computational domain. Obviously a fully self-consistent potential profile cannot be obtained for that outside region because that would amount to solving the same problem as we are addressing inside the domain. Instead, we must approximate the potential and then solve the orbit problem. The first approximation we make is to treat the potential as spherically symmetric. This will become exact in the large Debye length limit if the probe is an equipotential. Also, if the potential at the boundary is small, as it is in the case with short Debye length if r_b is not too small, it will again be spherically symmetric (because approximately zero). The angular distribution of reinjected flux, however, depends also on the radial profile of potential in the outside region. It involves the solution of orbits in a central force, the precise details of which depend on the radial potential dependence.

The natural choice for approximating the potential profile is the shielding form of equation (8). The direct calculation of the probability distributions with respect to velocity and position on the boundary $r = r_b$ does not appear to be analytically tractable even in a spherically symmetric potential. What is tractable, in part analytically, is to calculate the probability distributions of particles at infinity that will eventually reach the boundary, *and* to calculate the place where they hit the boundary, and their vector velocity there. This is sufficient to give the appropriate reinjection distribution by making the random choice at infinity and then reinjecting the particle at the corresponding phase–space location on the boundary.

In the orbit calculations of this and the next subsections, for notational convenience we write the potential normalized to T_i/Ze rather than T_e:

$$\chi \equiv \frac{\phi Ze}{T_i}, \tag{13}$$

where in this equation ϕ is the dimensional potential. In other words, expressed in terms of the normalized potential notation of the rest of the paper, $\chi \equiv \phi\,(ZT_e/T_i)$. Also the velocities are normalized to $v_n \equiv \sqrt{2T_i/m_i}$; specifically $u = v/v_n$ and $U = v_f/v_n$.

Take a Maxwellian distribution at infinity shifted by a drift velocity $v_f = Uv_n$. At infinity, ions that will eventually cross r_b must have velocity directed radially inward, so the direction of their velocity is a vector proportional to minus their position vector relative to the sphere centre as origin. Also they must have an impact parameter b that is less than $b_{\max} = (1 - \chi_b/u^2)^{1/2} r_b$. This limiting impact parameter may be derived immediately from energy and angular momentum conservation. If all such ions do in fact cross r_b (in other words if these conditions are sufficient as well as necessary) the external region is OML. The rate of collection of ions in the velocity element du from a distant solid angle element $\mathrm{d}\Omega$ is then

$$\mathrm{d}^2F = \frac{1}{\sqrt{\pi}}\, n_\infty v_n r_b^2 \exp(-[\boldsymbol{u} - \boldsymbol{U}]^2) \left(1 - \frac{\chi_b}{u^2}\right) u^3\, \mathrm{d}u\, \mathrm{d}\Omega. \tag{14}$$

Measuring polar angle, θ, of the velocity $\boldsymbol{u}$ relative to the direction of the drift velocity $\boldsymbol{U}$, and denoting its cosine by $c = \cos\theta$, the exponent here is $[\boldsymbol{u} - \boldsymbol{U}]^2 = u^2 - 2uUc + U^2$. Figure 1 illustrates the geometry of the orbit that is used throughout this section.

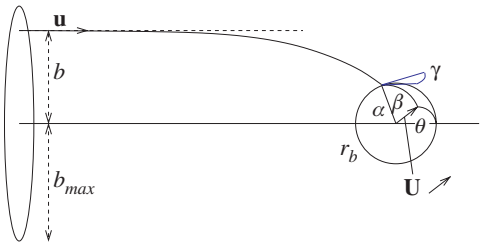

Figure 1. Geometry of collection orbit. The impact parameter b must be less than $b_{\max}$. The orbit reaches the boundary r_b at an angle α to its original direction, measured in the orbit plane. θ and β are the angles between the direction of the flow velocity ($\boldsymbol{U}$) and the original velocity ($\boldsymbol{u}$) and the impact position, respectively. γ measures the angle between the arc of β and the orbit plane.

The element of solid angle is

$$\mathrm{d}\Omega = 2\pi\,\mathrm{d}c. \tag{15}$$

Therefore, the flux distribution with respect to velocity at infinity, integrated over the entire sphere is

$$\begin{aligned}\frac{\mathrm{d}F}{\mathrm{d}u} &= 2\sqrt{\pi}n_\infty v_n r_b^2 \int_{-1}^{1} \mathrm{e}^{(-u^2-U^2+2uUc)}(1-\chi/u^2)u^3\,\mathrm{d}c \\ &= 2\sqrt{\pi}n_\infty v_n r_b^2 \frac{1}{2uU}\left[\mathrm{e}^{-(u-U)^2} - \mathrm{e}^{-(u+U)^2}\right]\left(1-\frac{\chi}{u^2}\right)u^3. \end{aligned}\tag{16}$$

The cumulative probability distribution in $c = \cos\theta$ is obtained by the same integral with an upper limit of c instead of 1. When normalized by the above expression, it can easily be shown to be

$$P_c(c) = \frac{\mathrm{e}^{2uUc} - \mathrm{e}^{-2uU}}{\mathrm{e}^{2uU} - \mathrm{e}^{-2uU}} \qquad -1 \leqslant c \leqslant 1. \tag{17}$$

The quantity $P_c(c)$ is the probability that a reinjected particle had $\cos\theta \leqslant c$ at infinity.

The cumulative distribution in velocity is then obtained by integrating $\mathrm{d}F/\mathrm{d}u$ with respect to u. Using a lower limit $u = u_0$ we get the total OML reinjected flux with velocity greater than u_0 at infinity in the form:

$$\begin{aligned}F(u > u_0) &= \sqrt{\pi}n_\infty v_n r_b^2 \frac{1}{U}\int_{u_0}^{\infty}\left[\mathrm{e}^{-(u-U)^2} - \mathrm{e}^{-(u+U)^2}\right](u^2-\chi)\,\mathrm{d}u \\ &= \sqrt{\pi}n_\infty v_n r_b^2 \frac{1}{U}\left\{\left(\frac{u_0+U}{2}\,\mathrm{e}^{-(u_0-U)^2} - \frac{u_0-U}{2}\,\mathrm{e}^{-(u_0+U)^2}\right)\right. \\ &\quad \left. + \left(U^2 + \frac{1}{2} - \chi_b\right)\frac{\sqrt{\pi}}{2}\left[\mathrm{erfc}(u_0-U) - \mathrm{erfc}(u_0+U)\right]\right\}. \end{aligned}\tag{18}$$

The cumulative probability distribution, i.e. the probability that a reinjected particle, at whatever angle, has velocity at infinity less than u_0, is then

$$P_u(u_0) = 1 - \frac{F(u > u_0)}{F(u > 0)} \qquad (0 \leqslant u_0 \leqslant \infty). \tag{19}$$

The process for reinjecting a particle is then as follows. (1) Choose a random velocity at infinity u from the cumulative probability $P_u(u)$. (2) Choose a random cosine of the angle at infinity, c, from $P_c(c)$, given u. (3) Choose a random impact parameter, b, from a uniform

distribution of b^2 from 0 to $b_{\max}^2$. (4) Choose the ignorable angles of the position and impact parameter from 0 to 2π. This specifies the reinjection at infinity.

The particle is then mapped to its corresponding position on the boundary r_b. To do this requires the calculation of the angle α in the plane of impact between the position of impact and the direction of the position at infinity (figure 1). This angle is obtained from the general solution for a central conservative force, which may be written:

$$\alpha = \int_0^1 \left[\frac{1}{s^2}\left(1 - \frac{\chi}{u^2}\right) - \xi^2 \right]^{-1/2} \mathrm{d}\xi, \tag{20}$$

where the integration variable is $\xi = r_b/r$ and $s \equiv b/r_b$. The integral is performed for each reinjection by a simple trapezoidal rule applied to the potential profile of equation (8) of which the two parts are precalculated on a uniform ξ-mesh. Only χ_b and a vary with time. The position on the boundary is obtained from α, and the velocity from the conservation of energy and angular momentum.

For the special case of an inverse square force ($\chi \propto 1/r$) the integral can be done analytically:

$$\cos\alpha = \frac{-(1 - \chi_b/u^2 - s^2)^{1/2} + (s + \chi_b/2u^2 s)(\chi_b/2u^2 s)}{1 + (\chi_b/2u^2 s)^2}. \tag{21}$$

This reinjection approach is computationally inexpensive, especially since $P_c(c)$ has a simple analytic inverse, but in view of its relative complexity and the possibility of coding errors, an independent cross-check seemed desirable. This was obtained by constructing a direct integral expression for the incoming flux density at r_b of ions from a shifted Maxwellian distribution. If β is the angle between the direction of drift velocity and the position on the sphere, the flux density there is

$$\Gamma(\beta) = n_\infty \left(\frac{m}{2\pi T_i}\right)^{3/2} \left(\frac{2T_i}{m}\right)^2 \int_0^\infty \int_0^{s_{\max}} \int_0^{2\pi} \exp(-\{u^2 + U^2 - 2uU[\cos\alpha\ \cos\beta + \cos\gamma\ \sin\alpha\ \sin\beta]\})\, \mathrm{d}\gamma\, s\, \mathrm{d}s\, u^3\, \mathrm{d}u, \tag{22}$$

where $s_{\max} = (1 - \chi_b/u^2)^{1/2}$ represents the maximum impact parameter collected. The γ integration arises from contributions from azimuthal angles around the radius vector. It can be carried out analytically to obtain

$$\Gamma(\beta) = \frac{2n_\infty v_n}{\sqrt{\pi}} \int_0^\infty \int_0^{s_{\max}} \mathrm{e}^{-(u^2+U^2)} u^3 \exp(2uU\cos\alpha\cos\beta)\, I_0(2uU\sin\alpha\sin\beta)\, s\, \mathrm{d}s\, \mathrm{d}u, \tag{23}$$

where I_0 is the modified Bessel function. It does not appear to be possible to integrate this expression further analytically, even in the case $\chi \propto 1/r$, equation (21). This perhaps explains why there does not seem to be a published treatment of this angular dependence of the collection flux of an inverse-square attracting sphere in a moving Maxwellian. Therefore, a program was written to perform the two-dimensional integral equation (23) numerically (for $\chi \propto 1/r$).

Excellent agreement (to about 0.2% with care) was obtained between the direct integration (23) applied to a collection sphere of radius $r = 1$, and the distribution of flux from the SCEPTIC code in the case $\lambda_{De} = 10^6$. This comparison verifies both the reinjection boundary condition and the integration of the particle orbits in the modelled region ($1 \leqslant r \leqslant r_b$) for a pure Coulomb field.

An additional check was performed by taking the potential from runs of SCEPTIC in which χ had been artificially symmetrized by averaging over angles. The reinjection routine was applied to that potential, but with $r = 1$ playing the role of r_b. Linear extrapolation in

$1/r$ to $r = \infty$ was required to complete the integral (20). A large number of reinjections (typically a few hundred thousand for reasonable statistics) was carried out and the position of the reinjections at infinity and at $r = 1$ was accumulated. The resulting distribution at infinity verifies that the random selection process is operating correctly. The distribution at $r = 1$ provides, in effect, a Monte-Carlo evaluation of the collection distribution using the fixed potential and the angular integration rather than the full particle orbit calculation. That this agrees with the distribution from the original SCEPTIC run is an independent verification of the orbit integrating part of SCEPTIC, for non-Coulomb potential profiles, indeed for just those potential profile shapes that are of interest (albeit spherically symmetrized).

3.3. Relationship between flux and density

In the simulation, the number of particles is specified and fixed. Therefore, instead of directly applying a boundary condition on the ion density, we need to determine the density at infinity consistent with this number of particles in the simulation region. In the quasineutral case of paper 1, it was not necessary to calculate n_∞ until the end of the calculation, but in this case, it is necessary to know the effective n_∞ at every step. Also, when the Debye length is long, the density at the boundary can be substantially different from n_∞, so the method of estimating it must be reasonably accurate. We cannot just use a simple extrapolation, as was done in paper 1.

We track the total number of reinjected particles at each step. This then tells us the flux of particles arriving from infinity (assuming that bound orbits are unpopulated). From this flux we deduce the density at infinity from the relationship between the average flux density and n_∞. For a spherically symmetric potential, the OML average flux arriving from infinity at r_b is (see equation (18) and cf [20])

$$F = F(u > 0) = 4\pi r_b^2 \frac{1}{4} n_{i\infty} v_n \left[\left(U + \frac{1 - 2\chi_b}{2U} \right) \mathrm{erf}(U) + \frac{1}{\sqrt{\pi}} \exp(-U^2) \right]. \tag{24}$$

In the limit $U \to 0$ this yields the more familiar OML expression for flux density $F/4\pi r_b^2 = (1/(2\sqrt{\pi}))n_\infty v_n(1 - \chi_b)$. Since with finite drift the potential is not symmetric (except in the limit $\lambda_D \to \infty$), we use here for χ_b the mean value of the potential of the reinjected particles, which is an appropriately weighted angular average.

The use of expression (24) provides an approximation to n_∞, given F, that is exact within the OML assumption in the limit of drift velocity zero or large ($U \ll 1$ or $U \gg \chi_b$), or large Debye length ($\lambda_D \gg r_b$).

The OML assumption that there are no intermediate effective potential barriers that reflect the particles and hence deplete parts of the inward orbit phase space, is not necessarily correct. Indeed it has been shown that it is never exactly correct for the large Debye length zero drift case [21]. However, our reinjection scheme enables us to calculate explicitly when an effective potential barrier is encountered. In fact we must do so, and reject such particles, for otherwise the orbit integrand (equation (20)) would become imaginary. If that happens we simply choose a new random particle at infinity and repeat the integration till we get a particle that penetrates. What we are therefore able to do is to track both the flux of particles injected at infinity F (including particles that are reflected before reaching r_b) and the flux of particles that penetrate to the boundary, F_b say. If the OML assumption is violated in the external region then $F_b < F$. But nevertheless, the relationship between F and n_∞ remains simply equation (24), which enables us to determine n_∞. Given that value, the depletion constant a, (equation (7)), can be evaluated, and the analytic shielding approximation for the succeeding step calculated.

4. Comparison with prior results

Although no rigorous calculations of the probe problem with flow have, to my knowledge, previously been published, a comparison with zero flow cases is a good test of the code. Comparison with approximate prior calculations with flow, and with experiments, helps to show the extent to which their results are affected by the approximations made.

4.1. Stationary plasma

The calculations of Laframboise [14, 15] provide comprehensive numerical values for flux to a spherical probe in a stationary plasma, over the range $\lambda_{De} = 0.01 - 5$, for various probe potentials, mostly for $T_i = T_e$. The results of SCEPTIC, run with zero flow, have been compared with that data at several probe potentials. For λ_{De} up to about 0.5 (times the probe size) SCEPTIC results using a domain size $r_{max} = 5$, give flux to the probe agreeing with Laframboise's results to within typically 0.2%. That uncertainty is approximately the accuracy claimed by Laframboise for his calculations and is also consistent with SCEPTIC's statistical uncertainty for total flux.

At the transition to OML behaviour ($\lambda_{De} \gtrsim 1$) however, numerically significant discrepancies are observed for the standard domain size. Figure 2 shows a comparison in this regime of the worst-case, most negative probe potential ($\phi_p = -25\, T_e/e$).

Two types of boundary condition in SCEPTIC are compared. The standard shielding solution approach, and a simpler approximation: taking the external potential to be $\propto 1/r$ for the purposes of reinjection. This second simpler approach enforces OML behaviour outside the computational domain and thus makes the total solution reach the OML limit ($26/\sqrt{2\pi} = 10.37$) prematurely unless r_{max} exceeds the radius where steep potential gradients exist, $\sim 3\lambda_{De}$. The shielding approach gives substantially better results when the domain size is limited, but discrepancies are removed entirely in the transition region only by increasing the computational domain size. This expedient was essential also for Laframboise, who used a domain r_{max} of 16.44 for $\lambda_{De} \geqslant 2$. The shielding approach gives discrepancies that are reduced by a factor of about three for $r_{max} = 5$ and negligible with $r_{max} = 10$. Incidentally, this result quantifies the recent theoretical redemonstration [22] that the deviations from OML are small in the long-Debye-length limit.

4.2. Flowing plasma

Perhaps the most comprehensive approximate calculations of flux to a sphere in a flowing plasma are contained in the thesis of Godard [23], the cylindrical parts of which were published later [24]. He took the potential surrounding the probe to be spherically symmetric. That is clearly incorrect but it allows the conservation of angular momentum to be used to reduce the problem's computational complexity. Godard used radial potential profiles calculated for the corresponding stationary plasma case by Laframboise's code. In a few cases, he plotted the angular dependence of the ion flux density to the probe.

Figure 3 shows a comparison of his results with those of SCEPTIC at drift velocity $v_f = \sqrt{2}$, which is the lowest non-zero velocity for which he gave angular results. For higher velocities one expects discrepancies to be less.

At very large values of λ_{De} the agreement is excellent to within draughtsmanship uncertainties, as it should be, since the potential is simply $\propto 1/r$ in this limit. For lower Debye lengths, where the plasma potential perturbation is substantial, the qualitative behaviour is correct but quantitative discrepancies of approximately 10–20% occur. These illustrate the

errors introduced by Godard's symmetry approximation. Since they are in opposite directions for the upstream and downstream sides, they would cause a significant fractional error, roughly twice as large, in the calibration factor of a Mach probe.

The total flux to the probe, as well as its spatial distribution, is also affected by flow and is tabulated in detail by Godard. Moreover, the total flux is the easiest quantity to measure experimentally. It is the main result of the experiments of Makita and Kuriki [25]. Figure 4 shows results from SCEPTIC for the total flux, expressed as an average flux density, compared with the approximate results of Godard, and the experiments of Makita and Kuriki.

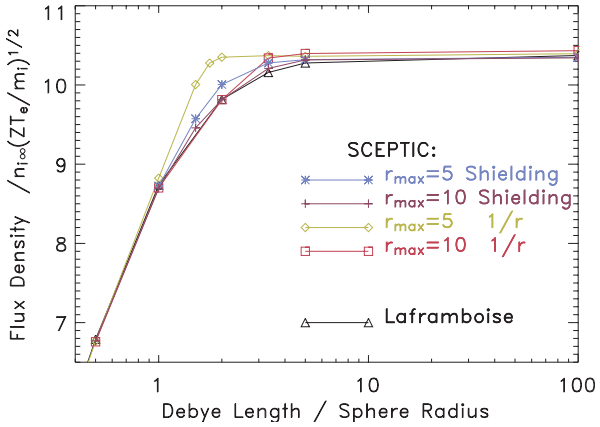

Figure 2. Comparison of fluxes in zero-flow calculations with corresponding results of Laframboise [14], for $\phi_p = -25$, $T_i = T_e$, with different computational domain size ($r_{\max}$) and with alternative treatments of the external potential.

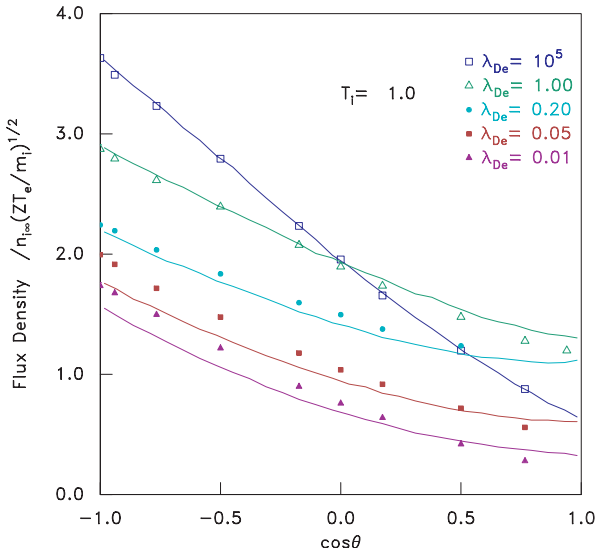

Figure 3. Variation of the flux density with position on the sphere, given as the cosine of the angle to the flow direction, for a flow $v_f = \sqrt{2}$, $T_i = T_e$ and various Debye lengths. The lines are SCEPTIC calculations and the points are taken from the approximate calculations of Godard [23].

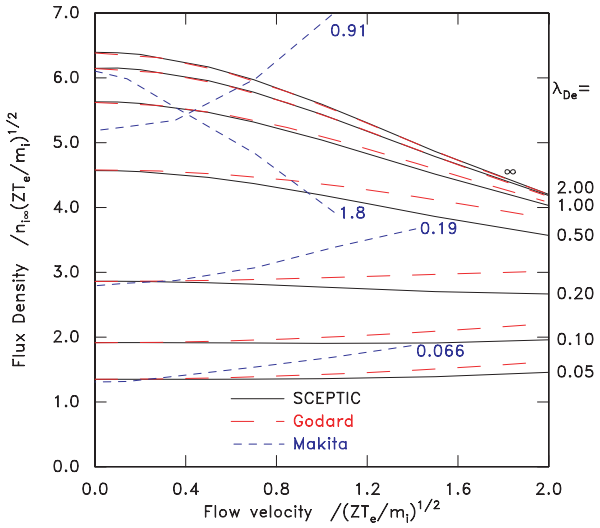

Figure 4. Comparison of flux (average flux density) from SCEPTIC (——) with calculations of Godard [23] (– – –) and experiments by Makita and Kuriki [25] (selected data trend indicated by short dashed line). Debye lengths relative to sphere size are indicated by labels. Here, $T_i = T_e$ and the probe potential is $\phi_p = -15\ T_e/e$.

As expected, Godard's calculations are in exact agreement with SCEPTIC if either flow is zero or $\lambda_{De} = \infty$. They deviate by over 10% at the higher flow velocities, when $\lambda_{De} < 1$.

Makita and Kuriki attributed the discrepancies between their experiments and the calculations of Godard to Godard's symmetry approximation. Figure 4 shows that this explanation of the discrepancies is incorrect. The SCEPTIC calculations fully include the asymmetric, self-consistent, potential variation but, if anything, they are further from the experiment than Godard's results. Therefore, the discrepancies must arise from other aspects of the experiments absent from both theoretical models.

5. Results

SCEPTIC calculates a full solution of the probe problem and the program can be obtained on the world wide web [26]. In systematizing the results, the difficulty lies in the number of free parameters. They are λ_{De}, ϕ_p, v_f, and T_i. Therefore, unlike the quasineutral case of paper 1, for which $\lambda_{De} = 0$ and ϕ_p is irrelevant, we have a four-dimensional parameter space. Moreover, the code provides a wealth of information about the plasma. In addition to the flux as a function of position on the sphere, it calculates the potential, density and velocity (indeed, distribution function) in the plasma region. The approach adopted here to presenting the results is, first, to show in a survey a few representative examples of cases with a variety of diagnostics, and then to give some more systematic summaries of the results covering the parameter space.

5.1. Plasma survey

Very crudely, the Debye-length dimension can be considered to be divided into three regimes: short, intermediate and long, corresponding to $\lambda_{De} \ll 1$, ~ 1, $\gg 1$, respectively. This proves to be the most important parameter governing the qualitatively different types of result. These

are then the examples we examine. The ion temperature (at infinity) is equal to the electron temperature unless otherwise indicated, and we will focus on a probe potential of -5 (T_e/e), which is in ion saturation slightly below the floating potential for most situations.

5.1.1. Intermediate Debye length. We begin with the most interesting but most difficult parameter regime, where the Debye length is of the order of the sphere radius. Figure 5 shows spatial distribution around the probe of the potential and density when $\lambda_{De} = 1$ and $v_f = 1$.

Radial profiles of the density for the same case are plotted in figure 6. The top frame is the density angle averaged, while the bottom frame plots densities at a range of angles. As

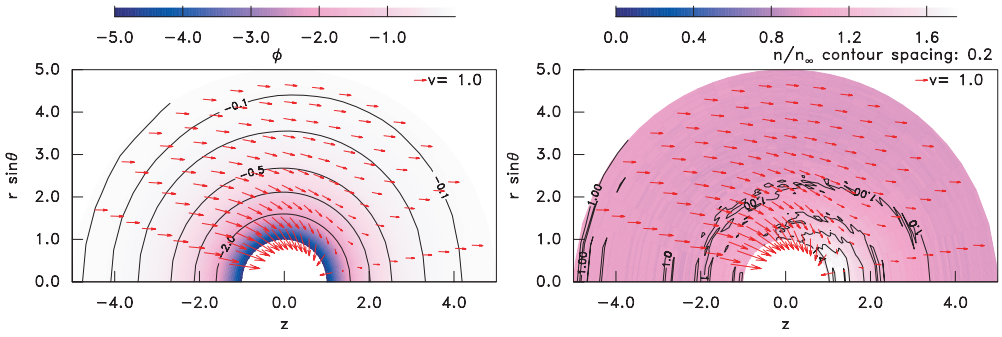

Figure 5. Potential and density contour plots ($\lambda_{De} = 1$, $T_i = 1$, $v_f = 1$, $\phi_p = -5$). The average ion velocity is indicated by the length of the vector arrows.

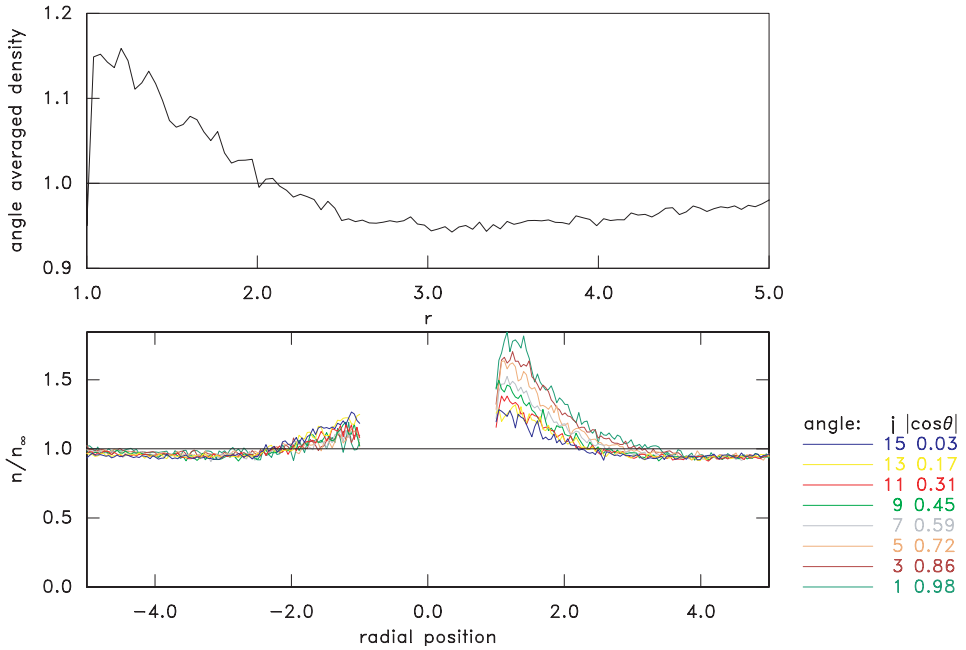

Figure 6. Density radial profiles for the same case as figure 5; top: angle averaged, bottom: along a range of angles whose cosine is specified in the legend. Negative position corresponds to negative $\cos\theta$, which is the upstream side.

we approach the sphere from the distant plasma, the density at first decreases slightly below its value at infinity. Then at about 2 to 2.5 times the sphere radius, it rises above n_∞. This bipolar behaviour is characteristic of the intermediate Debye length situation. Asymmetry in the density is substantial, the most pronounced effect being an enhancement on the downstream side, which is at first glance counterintuitive, since it corresponds to a density increase in the wake. It is not caused by asymmetry in the potential itself. The potential is almost spherically symmetric here, as can be seen in figure 5. Moreover, the code can be run with the potential artificially symmetrized by angle averaging, thus giving no angular acceleration. When that is done the downstream density increase remains.

The mean velocity of the ion distribution is indicated in figure 5 by arrows. At the edge of the computational domain, it is close to (but not exactly) the distant flow velocity. Influence of the attractive potential is seen to cause focusing of the ions behind the sphere causing a stagnation in the mean flow at about $r = 1.4$, near where the density is maximum.

Figure 7 shows radial profiles of the angle-averaged potential. The variation in potential arising from the different degrees of screening (that is different λ_{De}) is clearly seen. This potential plot has a much lower noise level than the density because of the smoothing effects of the Poisson equation at finite λ_{De}, and because this diagnostic is averaged over 40 steps. All the flux values given in this paper are averaged over many time-steps (typically 250–1000) and so correspond to much lower levels of density fluctuation than the instantaneous plots shown.

In figure 8 are shown the ion 'temperatures' around the probe. These are defined in terms of the second moment of the ion distribution function for velocity projected in the radial T_r or angular $T_\perp$ directions. The large rise of $T_\perp$ is a reflection of the velocity spread that arises from ions orbiting the sphere in opposite directions. They are accelerated in the attractive potential and so have larger energy than at infinity, leading to temperatures approaching the probe potential. The temperatures are higher on the downstream side, but still substantially enhanced upstream of the probe. There is some rise of T_r but not very much in this case.

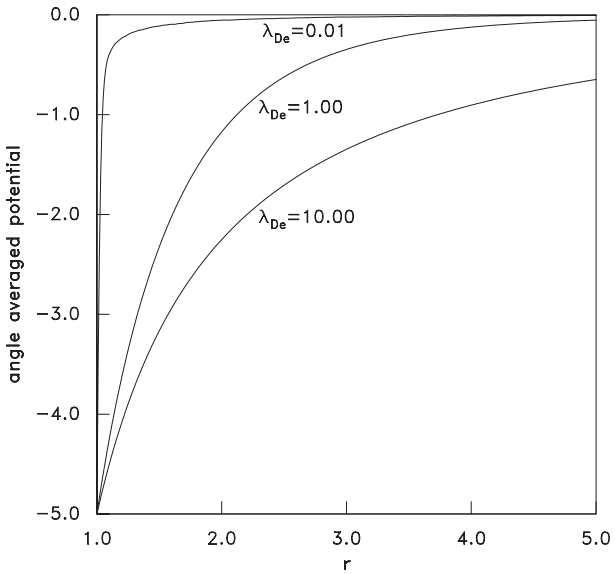

Figure 7. Angle-averaged ϕ-profile for three values of Debye length, all other parameters being equal ($T_i = 1$, $v_f = 1$, $\phi_p = -5$). The case $\lambda_{De} = 1$ corresponds to figure 5.

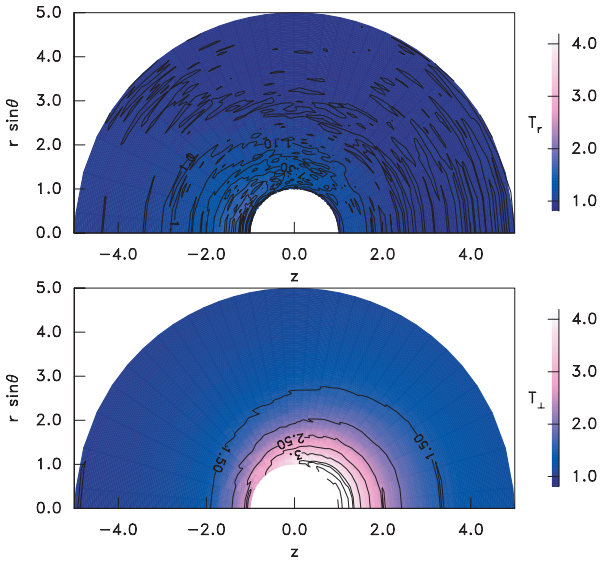

Figure 8. Contours of ion 'temperature' in the radial and angular directions for the same case.

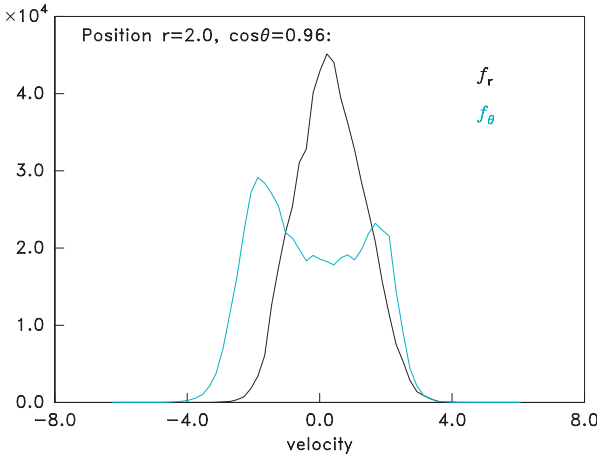

Figure 9. Distribution function of ions in a single cell in the downstream region. Units are simply particles per velocity bin, indicating the statistical uncertainty.

The code can, of course diagnose the ion distribution function directly. Figure 9 illustrates this in the downstream region, where the slightly two-humped nature of the tangential velocity distribution can be seen, confirming the orbital origin of the rise of the 'temperature'. It should be noted that a particle-kinetic treatment is obviously essential to embody this effect. No fluid model could do so. Fluid calculations such as those in references [27–29] can therefore not be regarded as sufficient to address quantitatively the physics of collisionless plasma flow past an object.

5.1.2. Long Debye length. In the limit of long Debye length, eventually the potential adopts a purely Coulomb form, since shielding becomes negligible. We illustrate the approach towards that limit with the case $\lambda_{De} = 10$. Figure 10 shows the radial density profiles. In this

case, they are all larger than n_∞ throughout. This unipolar behaviour and a reduction in spherical asymmetry are the main differences in the density distribution from the $\lambda_{De} = 1$ case (figure 5). The potential's angular distribution (not plotted here) for long Debye length is even more symmetric than the $\lambda_{De} = 1$ case (figure 5), as expected, and to the naked eye shows no variation with angle. The radial dependence is plotted in figure 7. The temperature variation is rather similar to figure 8.

5.1.3. Short Debye length. Since the limit of zero Debye length was treated in paper 1, we mention here only the issues of convergence that arise for $\lambda_{De} \ll 1$ but still finite. Difficulty arises because adequate finite difference solution of the Poisson equation requires the sheath to be resolved. The sheath is typically about 4 Debye lengths thick. So a mesh spacing less than approximately λ_{De} is required, forcing the radial mesh number to be $(r_{max} - 1)/\lambda_{De}$, for example 400 at $\lambda_{De} = 0.01$. When we push much beyond this mesh size, the number of particles per cell begins to drop to levels that are rather low and cause the statistical errors to be more problematic. Overcoming this difficulty in principle calls simply for more computational resources. However, it is known that because of the square-root singularity of the quasineutral case, the convergence of the flux to its value at $\lambda_{De} = 0$ is very slow. It is not explored in detail here.

The density profile in the case of small Debye length case is, like the potential profile (figure 7), monotonically decreasing towards the probe. The radial extent of the potential perturbation is greatly reduced.

5.2. Flux distributions

In figure 11, we show the flux density to the sphere as a function of the cosine of the angular position on the surface, $\cos\theta$. At high flow speed, the qualitative aspect meets the intuitive expectation that the downstream side ($\cos\theta > 0$) should receive less flux than the upstream. However, at low or moderate flow speed, this effect is almost absent in the low probe potential case ($\phi_p = -5$): there is hardly any asymmetry; and with high probe potential, ($\phi_p = -15$ for $v_f \lesssim 1.5$) the effect is reversed. That is, the downstream receives greater flux density than upstream. This result is quite contrary to the experience with infinitesimal Debye length reported in paper 1. It shows that the delicate balance between downstream density enhancement due to focusing, and radial velocity reduction due to the flow momentum, can be resolved in finite Debye length cases by the density enhancement overwhelming the velocity and causing downstream flux enhancement. The focusing is enhanced by higher (more negative) probe potential, which explains why reversal is more likely at $\phi_p = -15$, for example, than at $\phi_p = -5$.

In figure 12 are shown flux density versus angle for a wide range of Debye lengths at $\phi_p = -5$. The effects of focusing are most noticeable for the intermediate $\lambda_{De} = 0.1$ and 1 (figure 11) cases. At very large or very small λ_{De} more intuitive behaviour occurs. In all cases, a high enough flow velocity eventually causes the downstream flux to drop.

In figure 13 are shown two additional cases for higher probe bias $\phi = -15$, showing the quite strong focusing on the axis ($\cos\theta = 1$) for $\lambda_{De} = 0.1$, when the flow velocity is substantial. However, by the time the Debye length has reached 10 (in this case), the asymmetry inversion has disappeared. What this means is that the asymmetry reversal requires substantial penetration of the potential into the plasma to produce the focusing, but in addition a substantially shielded form. Unshielded Coulomb potential never gives rise to asymmetry reversal in the flux.

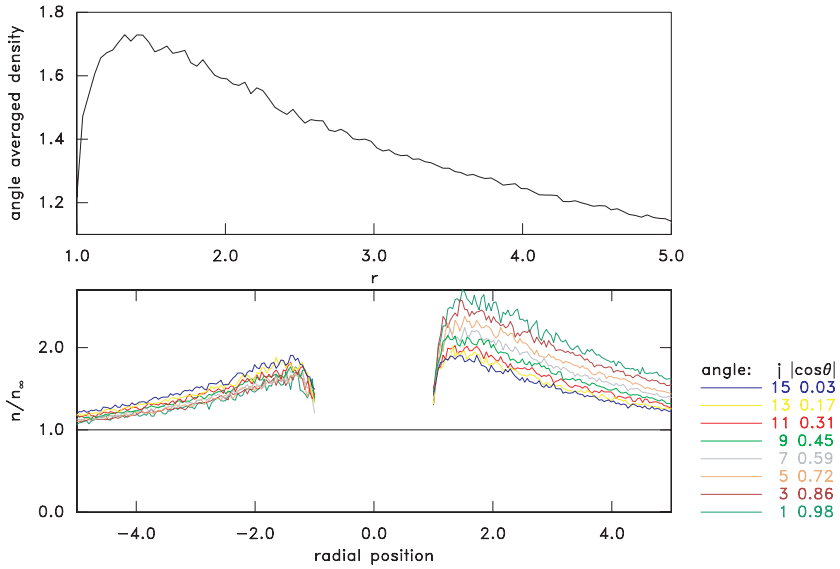

Figure 10. Density radial profiles for the case $\lambda_{De} = 10$, $v_f = 1$, $T_i = 1$, $\phi_p = -5$; top: averaged in angle, bottom: along a range of angles whose cosine is specified in the legend. Negative position corresponds to negative $\cos\theta$, which is the upstream side.

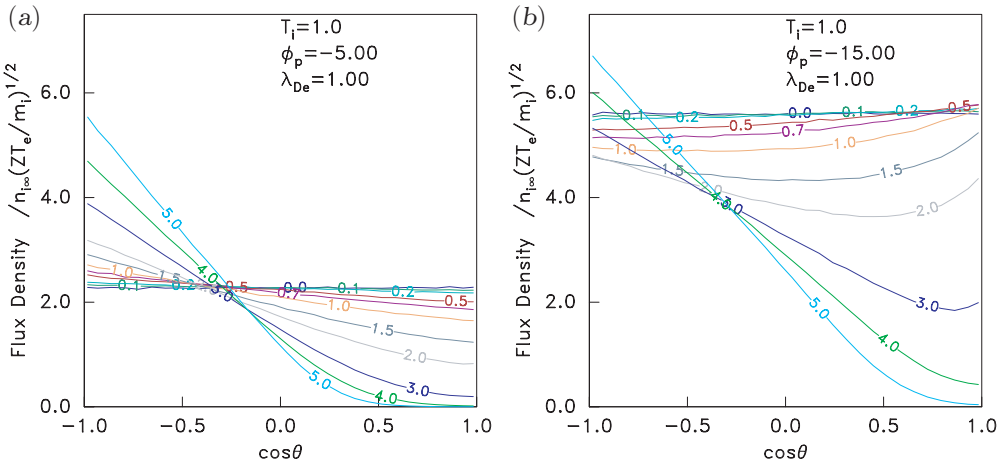

Figure 11. Flux density to sphere as a function of angle for various flow speeds at moderate (a) and high (b) potential bias; curves labelled with flow velocity (v_f) value.

When one investigates lower ion temperatures, the effects of the asymmetry reversal are much more serious. This is partly because of the reduction in the angular smoothing effect of the spread in ion velocity distribution. In figure 14 a case ($T_i = 0.1$, $\lambda_{De} = 3$) that has strong reversal over a range of velocities is shown. A potential contour plot for $v_f = 0.7$ is also shown to illustrate that the reversal is not caused by substantial asymmetry in the potential. The contours are only very slightly oblate. The asymmetry is caused by the velocity pattern induced by the potential. What is noticeable is that the mean velocity exhibits an eddy pattern (of the form of a 'smoke ring') slightly upstream of the sphere. This arises because substantial

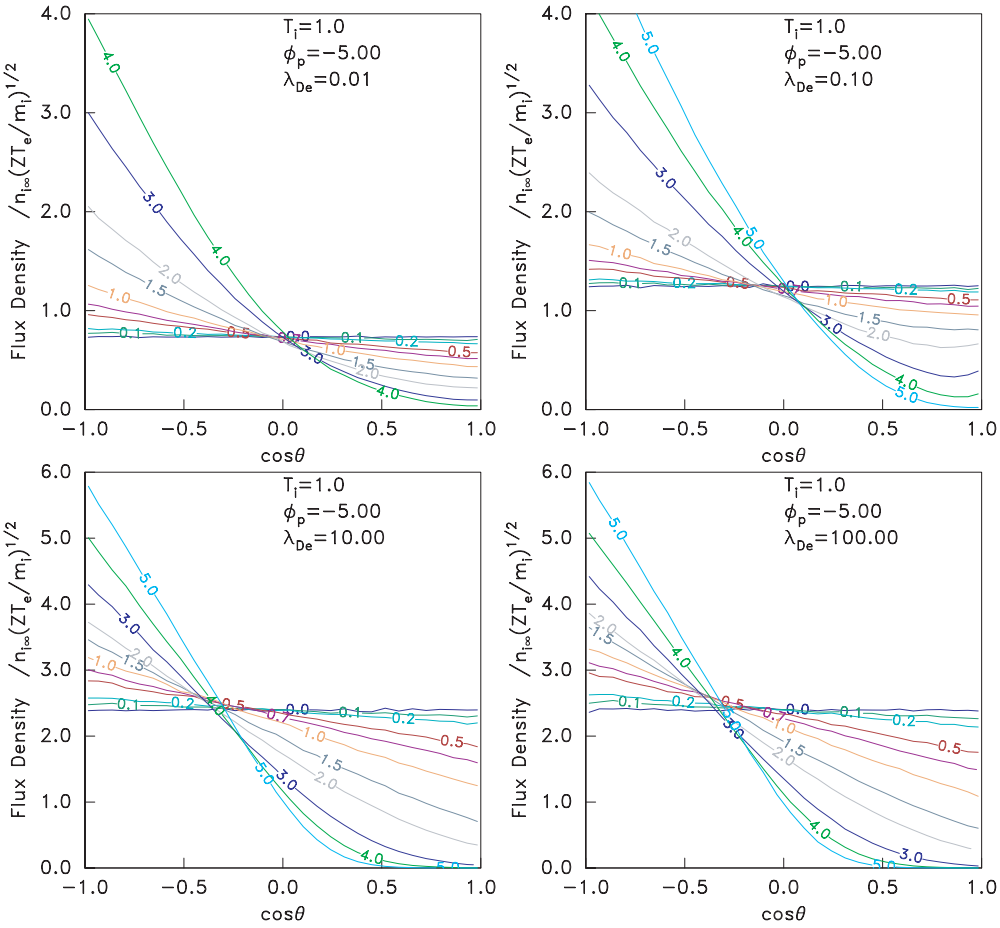

Figure 12. Flux density to sphere as a function of angle for probe potential $\phi_p = -5$ and various flow speeds; curves labelled with v_f value. Each plot is for a different Debye length.

numbers of ions with a fairly large impact parameter orbit the probe and are then directed in the opposite (upstream) direction close to the sphere after orbiting it by an angle of slightly less than 2π. In the partially shielded potential, these reversing orbits are not up–down symmetric parabolas as they would be for a Coulomb potential. (This calculation has been repeated with a larger domain size to verify that these qualitative effects are not caused by boundary conditions.)

The transition between enhanced and reduced downstream ion flux as flow velocity rises is produced by a detachment of the plasma at the downstream side at high enough velocity. This is illustrated by figure 15(a) showing colour contours of density. At this supersonic flow speed, the main density perturbation consists of an enhancement in the wake due to focusing. However, immediately behind the sphere ($r \lesssim 1.2$) the density drops precipitously, decreasing the downstream probe flux. What appears to happen is that this depleted region is inaccessible to most ion orbits because there is not enough acceleration to overcome the initial flow momentum. This is confirmed by the fact that the depletion occurs at a flow such that $2v_f^2 \gtrsim -\phi_p$. It is most visible in the contour plot of $T_\perp$ shown in figure 15(b). The high values of $T_\perp$, predominantly in the wake, are delimited by a cone. Within the cone,

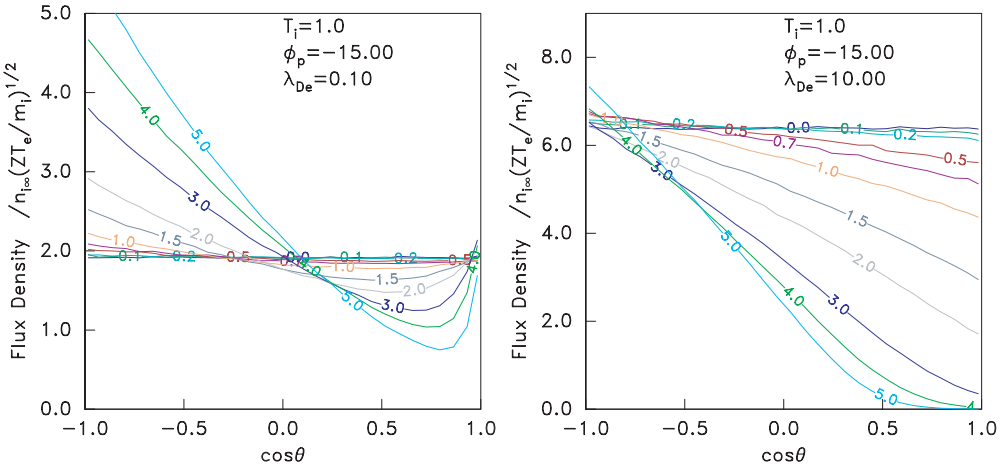

Figure 13. Flux density to sphere as a function of angle for strong negative bias, at various flow speeds; curves labelled with v_f value.

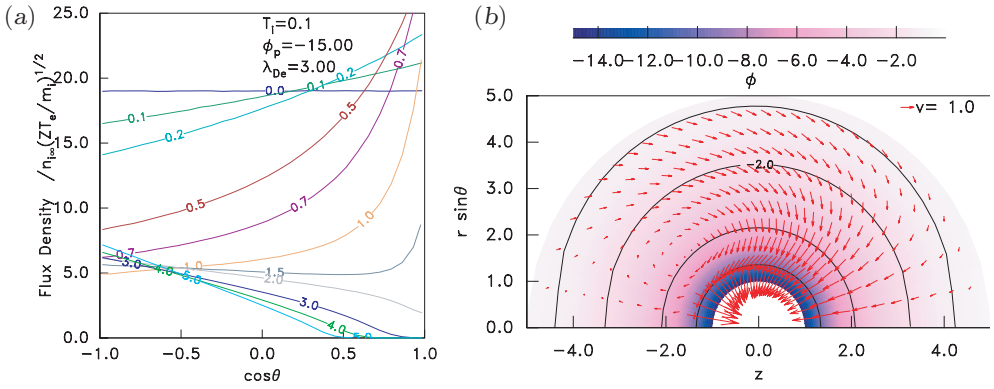

Figure 14. (*a*) Flux density to sphere as a function of angle for strong negative bias and low ion temperature. Curves labelled with v_f value. (*b*) Contour plot of potential for a case with deep asymmetry reversal ($T_i = 0.1, v_f = 0.7, \lambda_{\rm De} = 3, \phi_p = -15$) showing rather symmetric potential and mean velocity 'eddy'.

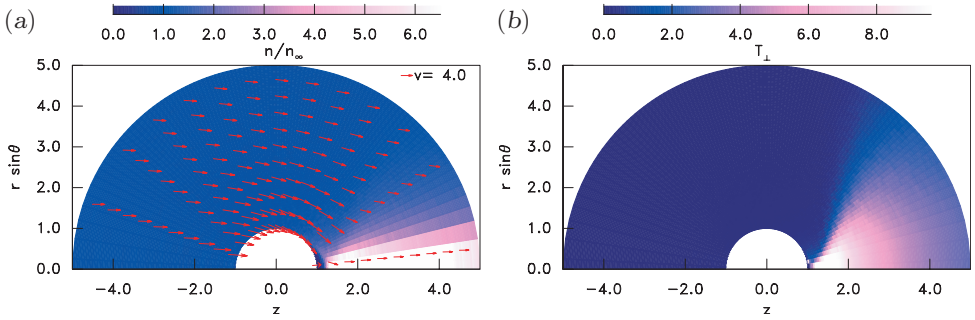

Figure 15. (*a*) Density contours showing detachment of the high density wake area from the probe surface at high flow velocity. (*b*) Tangential temperature contours showing the cone of overlapping streams where the effective temperature is high. $T_i = 0.1, v_f = 4, \phi_p = -15, \lambda_{\rm De} = 3$.

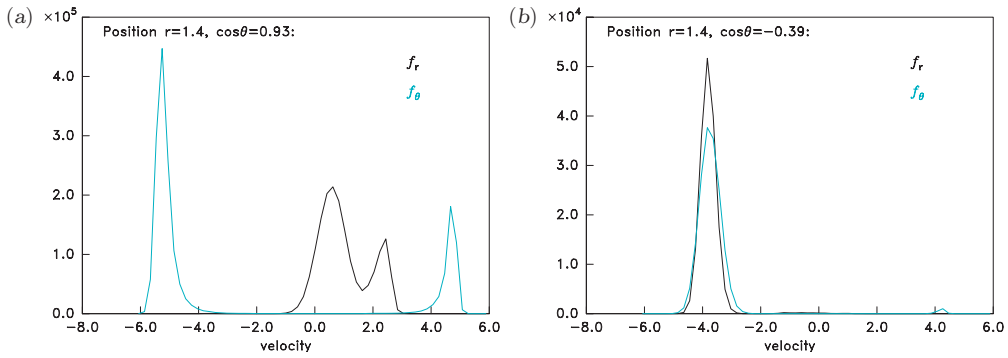

Figure 16. Distribution functions in the radial and tangential directions. (*a*) Within the trailing cone where two streams are present. (*b*) In the upstream region where only one stream is present. $T_i = 0.1$, $v_f = 4$, $\phi_p = -15$, $\lambda_{De} = 3$. Units of f are particle counts per bin, effectively arbitrary for physics purposes.

the high temperature is caused by the presence of two streams of ions which are orbiting in opposite directions around the probe. Outside the cone, there is no second stream. This is verified directly by diagnostics of the ion distribution function shown in figure 16. Detachment occurs when the cone angle becomes trailing, that is, there are no ions that scatter through more than 90°.

5.3. Flux ratios

The ratio of upstream to downstream ion flux density is used as a measure of flow velocity in Mach probe applications. In quasineutral plasmas (paper 1) and magnetized plasmas, it is found that the ratio, $R = \Gamma_u/\Gamma_d$ is approximately proportional to $\exp(K v_f)$. Therefore, we use, as a measure of the flux asymmetry, the quantity $\ln|R|/v_f$, which is effectively the value of K. (We use the flux density values at $\cos\theta = \pm 1$ in this ratio.) At low values of flow velocity, $\ln|R|/v_f$ certainly has a well defined limit which may be considered the small-velocity calibration factor. As figure 14 illustrates, however, for velocity greater than approximately unity, in other words supersonic flows, $\ln|R|/v_f$ is not at all constant. Moreover, this ratio does not capture all the detail of the angular variation of the flux density. Nevertheless it is a useful summary parameter.

A systematic study of the flux ratio has been carried out at $v_f = 0.5$. This value is chosen as small enough to give a reasonable approximation to the low-flow limit, but large enough that the ratio is not dominated by noise (as it is for much lower v_f). With this choice, a large number of SCEPTIC runs has been performed over a mesh in λ_{De} and ϕ_p, at chosen T_i.

Figure 17 shows a contour plot of $\ln|R|/v_f$ in the plane of probe potential and Debye length. It shows a trough deepening at larger probe potential with the minimum as a function of Debye length at about $\lambda_{De} = 0.5$. Its minimum value is negative for $-\phi_p \gtrsim 10$. At $\lambda_{De} = 0.01$ (along the bottom edge) the ratio factor is approximately 1, and is becoming independent of potential. However, it still has not reached the asymptotic value of 1.3 obtained in paper 1 for $\lambda_{De} = 0$. At long Debye length (along the top edge) the ratio still depends on probe potential, but has no negative regions.

At the lowest bias potential calculated, $\phi = -3$ (along the left-hand edge), which is typically approximately the floating potential, the ratio factor dips to approximately 0.65, which is half the quasineutral value. Thus, even minimizing the effects of finite Debye length

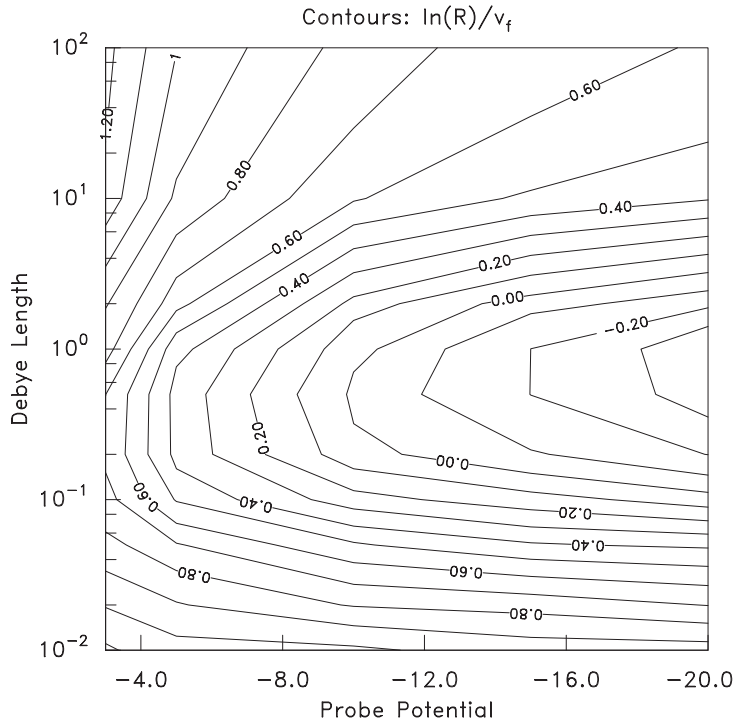

Figure 17. Flux-ratio contours for $T_i = 1$, $v_f = 0.5$.

by operating at minimal bias, does not provide a particularly reliable Mach probe calibration in the intermediate Debye length regime $\lambda_{De} \lesssim 1$.

Lower ion temperature makes all of these difficulties worse. This is illustrated by comparable data for $T_i = 0.1$ plotted as multiple curves in figures 18 and 19. The flux-ratio factor falls so quickly from its asymptotic value as λ_{De} increases that it changes sign at $\lambda_{De} \sim 0.1$ depending on ϕ_p and remains negative until $\lambda_{De} > 10$. What is more, even at $\lambda_{De} = 100$ the ratio is still well below its asymptotic value for $\lambda_{De} = \infty$.

5.4. Deferred investigations

While this paper has focused on the ion collection flux density for an equipotential probe, SCEPTIC can, with minor modification, also address other related problems of interest, which are deferred here. These include the self-consistent potential distribution on an insulating probe and the surrounding plasma perturbation, the surface electric field and the total drag force on a spherical particle, and more specific cases than could be covered in a single paper.

6. Conclusions

The SCEPTIC code gives a comprehensive solution to the problem of the interaction of a sphere with a flowing collisionless plasma. It transpires that the asymmetry of the plasma potential, while noticeable, is neither large nor a dominant effect. Nevertheless, a remarkable new effect has been documented, namely the reversal of the asymmetry of the collection flux at values of the Debye length of the same order of magnitude as the probe radius. The enhancement of

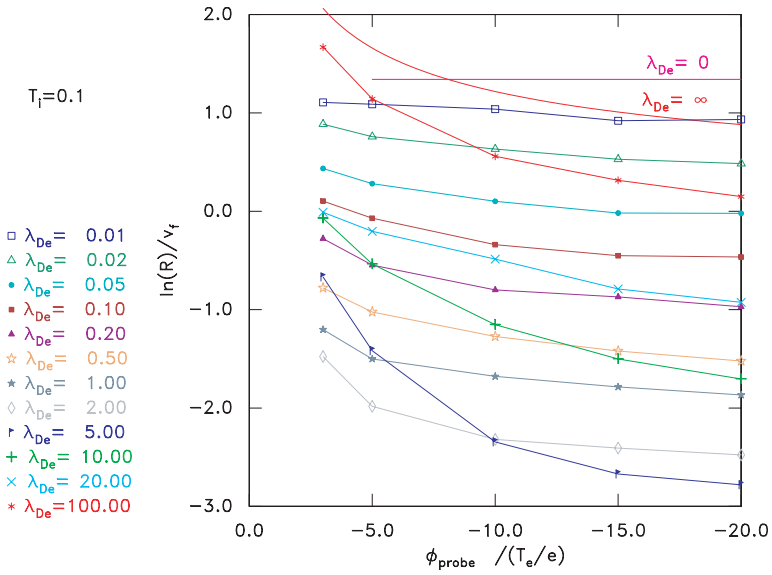

Figure 18. Flux ratio versus probe potential for a wide range of Debye lengths, $T_i = 0.1$, $v_f = 0.5$. The asymptotic values for $\lambda_{De} = 0$ (from paper 1) and $\lambda_{De} = \infty$ (from the direct integration equation (23)) are also shown as lines without points.

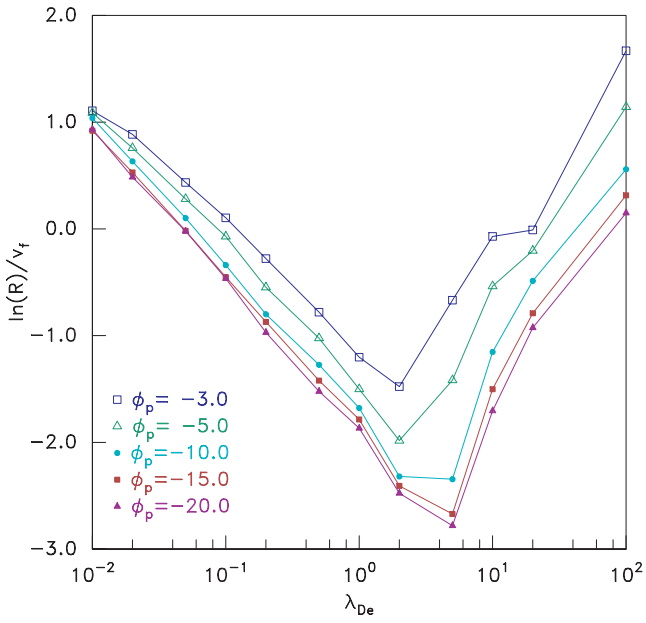

Figure 19. Flux ratio versus Debye length for a range of probe potentials, $T_i = 0.1$, $v_f = 0.5$.

collection on the downstream side is due to focusing of the ions by the potential surrounding the probe. But purely Coulombic $(1/r)$ potential variation does not produce flux asymmetry reversal. It occurs only when there is substantial plasma shielding of the potential. As the flow velocity increases, eventually the reversal disappears, quite abruptly, as the high density wake detaches from the back of the sphere. This detachment is predominantly an orbit effect.

Unfortunately, since even the direction of flux density asymmetry is dependent on the values of the Debye length and the ion temperature, the results show how problematic is the use of upstream/downstream flux asymmetry to a spherical probe as a measure of flow, when the Debye length is a significant fraction of the probe size. It is probable that different geometries might show less susceptibility to the reversal of flux asymmetry. But the orbit effects that cause the enhancement of density in the wake will be present for any object of limited extent. Therefore, a reliable Mach probe configuration may be difficult or impossible to design, and certainly would need detailed modelling to validate theoretically.

Acknowledgments

The calculations reported here were performed on the Alcator Beowulf cluster which is supported by US DOE grant DE-FC02-99ER54512.

Appendix. Accuracy

The minimum statistical fractional uncertainty associated with the total flux is approximately $1/\sqrt{N}$, where N is the total number of collected particles used for calculating the flux. This is the Poisson statistics level for uncorrelated particles. Correlation could increase the fluctuations. For typical SCEPTIC runs reported here, $N = 10^6$ or more, so that the statistical uncertainty is small, $\sim 10^{-3}$. Even for individual angular elements, which collect, for example, 30 times less particles, the statistical uncertainty is less than 1%. Typically issues of convergence are more important.

At intermediate values of Debye length, $\lambda_{De} \sim 1$, as shown in figure 2, full convergence requires the domain to be larger than the standard size $r_{max} = 5$. Moreover, it is observed that flowing plasmas, particularly those with low ion temperature, are more susceptible to the finite domain approximations than is indicated in figure 2. It is computationally expensive to increase the domain size because the flux of particles collected is inversely proportional to r_{max}^3. The statistical uncertainties thus rise $\propto r_{max}^{3/2}$. A related problem is that it takes longer for particles to cross a larger domain, so that the number of time-steps to convergence increases with domain size. To establish how large a domain is really necessary some moderately

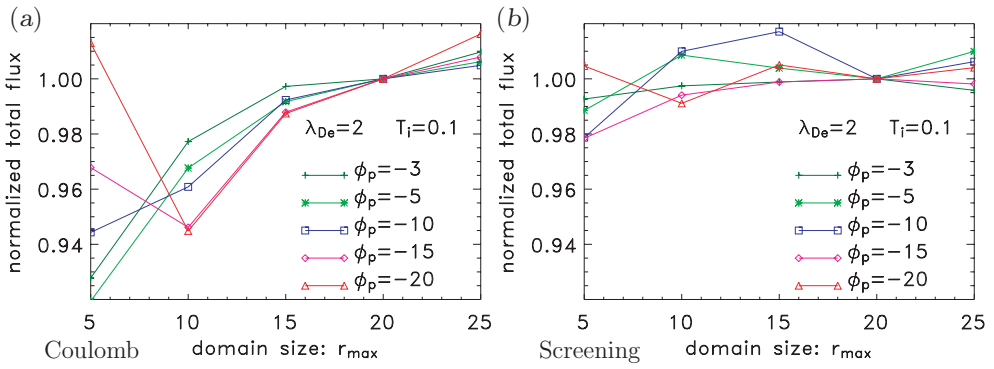

Figure 20. Convergence of the total flux to the sphere, normalized to its observed value when $r_{max} = 20$, as a function of computational domain size, keeping the radial cell size constant. Flow velocity is 0.5. Reinjection is governed by an external potential that is (*a*) of Coulomb form $\propto 1/r$, or (*b*) of the screening form, equation (8).

expensive cases have been run with a range of domain sizes. Figure 20 shows a convergence test for some of the most challenging parameters, with radial cell size approximately constant ($\sim$0.04), and 30 angular cells. The errors are about 10% at $r_{\max} = 5$ for the simplified external potential form $\propto 1/r$. The screening treatment that is standard in SCEPTIC reduces it to $\lesssim$2%. For essentially all experimental purposes that is sufficient. At the highest values of $r_{\max}$, statistical fluctuations in the density are beginning to be significant, which shows that there is little advantage in increasing the domain size for these parameters. When T_i is higher, the convergence errors are substantially less.

Corrigendum

Tables A5, A6, and A7 of paper 1 were affected by an error in postprocessing. The flux density values presented are 3.3% lower than they should be. All other tables and figures are correct. None of the conclusions is affected.

References

[1] Hutchinson I H 2002 *Plasma Phys. Control. Fusion* **44** 1953
[2] Hutchinson I H 1988 *Phys. Rev.* A **37** 4358
[3] Chung K-S and Hutchinson I H 1988 *Phys. Rev.* A **38** 4721
[4] Hutchinson I H 2002 *Principles of Plasma Diagnostics* 2nd edn (Cambridge: Cambridge University Press)
[5] Shats M G *et al* 1997 *Phys. Plasmas* **4** 3629
[6] Solomon W M and Shats M G 2001 *Rev. Sci. Instrum.* **72** 449
[7] Shinohara S, Matsuoka N and Matsuyama S 2001 *Phys. Plasmas* **8** 1154
[8] Hsu S C *et al* 2001 *Phys. Plasmas* **8** 1916
[9] Hudis M and Lidsky L M 1970 *J. Appl. Phys.* **41** 5001
[10] Hutchinson I H 2002 *Phys. Plasmas* **9** 1832
[11] Allen J E 1992 *Phys. Scr.* **45** 497
[12] Nitter T 1996 *Plasma Sources Sci. Technol.* **5** 93
[13] Cosmo M L and Lorenzini E C 1997 *Tethers In Space Handbook Smithsonian Astrophysical Observatory* (Cambridge) 3rd edn, http://cfa-www.harvard.edu/ spgroup/handbook.html
[14] Laframboise J G 1966 Theory of spherical and cylindrical Langmuir probes in a collisionless Maxwellian plasma at rest *Technical Report* 100 University of Toronto Institute for Aerospace Studies
[15] Laframboise J and deLeeuw J H (ed) 1966 *Rarified Gas Dynamics: Proc. 4th Int. Symp. (Toronto)* vol 2 (New York: Academic) p 22
[16] Press W H, Flannery B P, Teukolsky S A and Vetterling W T 1989 *Numerical Recipes* (Cambridge: Cambridge University Press)
[17] Birdsall C K and Langdon A B 1991 *Plasma Physics via Computer Simulation* (Bristol: Institute of Physics Publishing)
[18] Hockney R W and Eastwood J W 1988 *Computer Simulation Using Particles* (Bristol: Institute of Physics Publishing)
[19] Al'pert Ya L, Gurevich A V and Pitaevskii L P 1965 *Space Physics with Artificial Satellites* (New York: Consultants Bureau)
[20] Northrop T G 1992 *Phys. Scr.* **45** 475
[21] Allen J E, Annaratone B M and de Angelis U 2000 *J. Plasma Phys.* **63** 299
[22] Lampe M 2001 *J. Plasma Phys.* **65** 171
[23] Godard R 1975 A symmetrical model of cylindrical and spherical collectors in a flowing collisionless plasma *PhD Thesis* York University Toronto, Ontario
[24] Godard R and Laframboise J G 1983 *Planet. Space Sci.* **31** 275
[25] Makita H and Kuriki K 1978 *Phys. Fluids* **21** 1279
[26] from http://silas.psfc.mit.edu/sceptic/sceptic.tar.gz
[27] Stangeby P C and Allen J E 1971 *J. Plasma Phys.* **6** 19
[28] Grabowski R and Fischer T 1975 *Planet. Space Sci.* **23** 287
[29] Melandso F and Goree J 1995 *Phys. Rev.* E **52** 5312